# Certified Reduced Basis Method in Geosciences

## Addressing the challenge of high dimensional problems

**Denise Degen · Karen Veroy · Florian Wellmann**

Received: date / Accepted: date

**Abstract** One of the biggest challenges in Computational Geosciences is finding ways of efficiently simulating high-dimensional problems. In this paper, we demonstrate how the RB method can be gainfully exploited to solve problems in the Geosciences. The reduced basis method constructs low-dimensional approximations to (high-dimensional) solutions of parametrized partial differential equations. In contrast to other widely used geoscientific reduction techniques, the reduced basis method reduces the Galerkin approximation space, and not the physical space and is consequently much less restrictive. Another advantage of the method is that for the problems considered in this paper, the method provides a bound to the error in the reduced order approximation, thus permitting an objective evaluation of the approximation quality. Using a geothermal conduction problem we demonstrate that depending on the model we obtain a maximum speed-up of three orders of magnitude with an approximation error that is very small in comparison to typical measurement errors. This significant reduction of the cost of the forward simulation allows performing uncertainty quantification, inversions, and parameter studies for larger and more complex models than currently possible.

**Keywords** Model Order Reduction · Reduced Basis Method · Finite Element Method · Geothermal Conduction · MOOSE Framework

D. Degen
Aachen Institute for Advanced Study in Computational Engineering Science (AICES) &
Computational Geoscience and Reservoir Engineering (CGRE)
RWTH Aachen University
Schinkelstraße 2, 52062 Aachen
Tel.: +49(0)241 80 99 147
Fax: +49(0)241 80 628 498
E-mail: degen@aices.rwth-aachen.de

K. Veroy
Aachen Institute for Advanced Study in Computational Engineering Science (AICES)
Faculty of Civil Engineering
RWTH Aachen University
Schinkelstraße 2, 52062 Aachen

F. Wellmann
Computational Geoscience and Reservoir Engineering (CGRE)
RWTH Aachen University
Wüllnerstraße 2, 52072 Aachen

## 1 Introduction

In the Geosciences, the ability to provide accurate predictions of subsurface processes can have a significant societal impact since it enables more efficient management, and sustainable use of valuable resources. Therefore, the field of Geosciences aims at gaining an accurate understanding of the spatial distribution of the earth's subsurface properties, and of the involved physical processes, such as fluid and heat transport, chemical species transport, and mechanical processes.

With the use of model order reduction (MOR) we can potentially gain a significant speed-up for the simulations while retaining a predefined level of accuracy. This is of great importance since a meaningful prediction presents us with two main challenges. First, complex coupled processes have to be analyzed over a large spatial and temporal domain. Additionally, the highly heterogeneous nature of the subsurface typically results in a high dimensional parameter space leading to the so-called "curse of dimensionality". Hence, the encountered tasks are computationally intensive and expensive, thus typically requiring high-performance-computing (HPC) infrastructures [5], [7], [10]. Second, retrieving information from the subsurface is a non-trivial process due to, for instance, limited access to the areas of interest. Consequently, the measurements are associated with high uncertainties [9], [42]. Accounting for these

uncertainties requires numerous simulations, which are often prohibitively expensive when using standard approaches such as the finite element (FE) method.

As a step towards addressing these challenges, we employ a particular MOR technique, the reduced basis (RB) method, which computes low-dimensional approximations to solutions of parametrized partial differential equations. The RB method is especially beneficial in the many-query or real-time context, for instance, in uncertainty quantification, inversion, and sensitivity analysis where many forward simulations are required to obtain meaningful results. The RB method, however, is not suitable for *single* high precision simulations because of the offline construction time of the reduced space. Consequently, the method pays off only after a certain amount of simulations [16], [31], [33], as illustrated in Section 5.

To overcome the "curse of dimensionality", many geoscientific applications are focused solely on the area of interest, and with spatial and temporal discretizations that are coarse enough to permit computation in a reasonable time. However, such approaches neglect possibly significant influences from regions outside the area of interest. Furthermore, attempts to compensate for such effects through special boundary conditions often result in insufficient descriptions of the actual problem, and similar problems occur for coarse spatial and temporal discretizations because one needs to have methods that correctly upscale the properties from smaller to larger scales. Most of the methods used in Geosciences for reducing the dimensionality directly reduce the physical spatial and temporal domain by taking fewer data. In this paper, we propose an alternative approach in which we systematically reduce the dimensionality without resorting to a priori – possibly false – assumptions. As previously mentioned, the RB method further provides an error estimate, permitting an objective, qualitative evaluation of our approximation. This error bound, as mentioned in Section 2, allows an efficient construction of the RB space. Further information about how to optimally use the error bound in Geosciences follows in Section 5.

We present an application, namely the DwarfElephant package, to the Multiphysics Object-Orientated Simulation Environment (MOOSE) [36], implementing the RB method. MOOSE, primarily developed by the Idaho National Laboratory, offers a built-in parallelization. The framework builds upon the libMesh [23] and PETSc [3] libraries. The RB implementation mainly uses the rbOOmit package [24] provided by libMesh. A built-in parallelization is especially advantageous since constructing parallelized problems for HPC infrastructures is often anything but trivial. For further details regarding the software packages, refer to Section 3.

The RB method was thoroughly studied and presented by, for instance, [13], [16], [31], [33] and used in applications such as the medicine [22]. However, it is fairly unknown in the field of Geosciences. So far, the applications of reduced order modelling in the Geosciences has been largely limited to the use of Proper Orthogonal Decomposition (POD), e.g. for thermal [35] and groundwater studies [12], [34]. However, compared to the RB method, POD has the disadvantage of being less efficient for a large number of parameters [21], [41].

Consequently, this paper aims at introducing the RB method to the geoscientific community. We are therefore using simplified benchmark problems to better illustrate the concepts of the method. The goal of this paper is not to further develop the mathematical methodology, but instead to demonstrate the advantages of the method for geoscientific applications by using motivating and well-known examples within the geoscientific community. The fact that this link is missing so far becomes clear when considering that the method, although available for nearly 20 years, has, to our knowledge, not been widely used in geoscientific problems. Some papers as, for instance, [1] and [26] are using the same PDEs as the geoscientific applications, but the papers are focused on the methodology and are not applying it to realistic basin-scale models. We further aim to allow a better usability of the method by incorporating it into a software, the MOOSE framework, that is already known and widely used in the community [18], [30]. A detailed description of the software is found in Section 3. In addition, we demonstrate the extension of the method to complex basin-scale geothermal models (see Section 4). However, we will not discuss the geological implications of these simulations in detail since this is beyond the scope of this paper.

We evaluate the performance of the RB method for geoscientific applications. Several software packages are available for the RB method:

- rbMIT [17],
- RBmatlab [37],
- rbOOmit [24],
- pyMOR [28],
- Feel++ [32],
- FreeFem++ [14],
- RBniCS [4], [16].

However, some of these packages, e.g. the MATLAB packages rbMIT and RBmatlab, are based on proprietary software, making it difficult to provide results that are openly verifiable and reproducible. Furthermore, they often lack high-performance capabilities, thus making them unsuitable for large-scale models. Other packages, such as pyMOR and libMesh, are constructed as libraries. Thus, a lot of work is required for setting up a specific problem. Python wrappers are only available for pyMOR, RBnicS, and FreeFem++. Some of these libraries are used by higher-level software environments, for example, RBniCS uses FEniCS (`http://fenicsproject.org/`) and MOOSE is based on libMesh, which contains the rbOOmit package. So, with the DwarfElephant package, we provide an easy, and open source access to the RB method taking full advantage

of the user-friendly MOOSE environment, allowing an easy set-up of new models and a quite straightforward approach to further extend the package.

Additionally, MOOSE applications have been used in several previous geophysical studies [18], [19], [29], [30]. Our package thus offers a direct use of the RB method, and allows a merging with already existing MOOSE applications, something that is not possible with any of the other presented packages. Although this paper focuses on geoscientific applications, the package is constructed in a general fashion enabling a usability independent of the application field.

The theoretical background of the RB method is explained in Section 2. We demonstrate this promising methodology by using a geothermal energy application, which requires numerical forward simulations (Section 3). Furthermore, we show the performance of the package in comparison to the standard FE method. All results are presented in Section 4 followed by a discussion of the results in Section 5. Section 6 concludes this paper by giving an outlook about how the obtained speed-ups can, in turn, be used in, for instance, sensitivity and uncertainty analyses or in the solution of other inverse problems.

## 2 The Reduced Basis Method

As previously mentioned, the RB method is, so far, not widely used in the Geosciences. We thus present the theoretical background in greater detail to offer a brief overview of the method itself. In addition, we provide a geoscientific example to illustrate the methodology in a geoscientific context.

In general, the RB method is independent of the discretisation scheme; however, since MOOSE [36] is a FE solver, we explain the background of the RB approach by considering a FE problem. For $\mu \in \mathbf{D}$ - where $\mathbf{D}$ is the parameter domain in $\mathbb{R}^P$ (with $P$ being the number of parameters) - find $u(\mu) \in X$ that satisfies [16], [31], [33]:

$$a(u(\mu), v; \mu) = f(v; \mu), \qquad \forall v \in X. \tag{1}$$

Here, $a$ is an affine parametric bilinear form and is dependent on the parameter $\mu$. Both the variable $u$, for which we are solving, and the test function $v$ are in the function space $X$ ($H_0^1(\Omega) \subset X \subset H^1(\Omega)$), and $\Omega$ is the spatial domain in $\mathbb{R}^3$. The functional $f$ is an affine parametric linear form on $X$ and is dependent on the parameter. Given $u(\mu)$, we evaluate the output of interest $s(\mu)$ [16], [31], [33]:

$$s(\mu) = l(u(\mu); \mu). \tag{2}$$

Here, $l$ is an affine linear form on $X$. It is a linear functional that connects the input $\mu$ to the output through our field variable $u$. Hence, in the context of Geosciences it can be seen as a specific type of post-processor.

We further assume that all linear and bilinear forms are affine parameter-dependent, i.e, they can be expressed as a sum of terms that are comprised of a parameter-dependent and a parameter-independent part [16], [31], [33].

$$l(v; \mu) = \sum_{q=1}^{Q_l} \theta_l^q(\mu)\, l^q(v), \qquad \forall v \in X, \forall \mu \in \mathbf{D}, \tag{3}$$

$$f(v; \mu) = \sum_{q=1}^{Q_f} \theta_f^q(\mu)\, f^q(v), \qquad \forall v \in X, \forall \mu \in \mathbf{D}, \tag{4}$$

$$a(w, v; \mu) = \sum_{q=1}^{Q_a} \theta_a^q(\mu)\, a^q(w, v), \qquad \forall v, w \in X, \forall \mu \in \mathbf{D}. \tag{5}$$

Here, $w$ is the trial function and $\theta$ the parameter-dependent term of the PDE.

For a geoscientific context this decomposition can be easily understood by inspecting, for instance, the simplest form of a geothermal conduction problem governed by the following PDE:

$$\lambda \nabla^2 T = 0 \qquad \text{in } \Omega \tag{6}$$

In this case, we consider a steady-state problem without any source or sink terms, where $\lambda$ denotes the thermal conductivity, $T$ the temperature, and $\Omega$ our domain. Furthermore, we apply a Dirichlet boundary condition at the top of the domain and a Neumann boundary condition with the boundary value $e$ at the bottom.

Taking the PDE (6) into account, considering the compliant case (i.e, where $f = l$), and setting $\theta_f^q(\mu)$ and $Q_f$ to 1, it follows that:

$$f(v) = \int_\Gamma v\, e\, d\Gamma \qquad \forall v \in X, \tag{7}$$

Here, $\Gamma$ is the boundary in $\mathbb{R}^2$ and $e$ is the boundary value. Furthermore, we define $\theta_a^q(\mu)$ equal $\mu^q$ equal $\lambda^q$, where $\mu_q$ defines any parameter in the respective layer, $\lambda^q$ denotes the thermal conductivities for the respective layers, and $\Omega_q$ is the integration volume. We can therefore write:

$$a(w, v; \lambda) = \sum_{q=1}^{Q_a} \lambda^q \int_{\Omega_q} \nabla w \nabla v\, d\Omega_q \quad \forall v, w \in X, \forall \lambda \in \mathbf{D}. \tag{8}$$

As seen in (8), $a$ contains a parameter-dependent and -independent part. For a thermal conduction problem, the diffusive part of the equation is always the same, only the thermal conductivity is varying for different rock types. That does not mean that both parts can be evaluated independently of each other. Following (8), the thermal diffusion term ($\nabla^2 T$) is the parameter-independent part of the PDE, whereas the thermal conductivity ($\lambda$) is the parameter-dependent part. In contrast to the Dirichlet boundary conditions, Neumann and Robin boundary conditions appear in

the integral form and are generally dependent on the parameter. In our specific example, however, we consider a parameter-independent Neumann boundary condition only (7).

To sum up, for a geothermal conduction example consisting of three layers (two shale layers interrupted by a sandstone layer; i.e, $Q_a = 3$), where we want to vary the thermal conductivity in each of these layers we end up with three $A_q$. Considering a homogeneous Dirichlet boundary condition and a Neumann boundary condition for the top and bottom of the model, respectively, we have one $F_q$. Note that the decomposition into the different layers can be automatically performed by the DwarfElephant package, for further details refer to Section 3.

For this paper, we consider that $f$, $l$, and $a$ are continuous on $X$ (9). We further assume that $a$ is symmetric and parametrically coercive (10) [16], [31], [33].

$$\gamma(\mu) = \sup_{w\in X}\sup_{v\in X}\frac{a(w,v;\mu)}{\|w\|_X\|v\|_X} < \infty \qquad \forall\mu\in\mathbf{D} \tag{9}$$

$$\alpha(\mu) = \inf_{w\in X}\frac{a(w,w;\mu)}{\|w\|_X^2} > 0 \qquad \forall\mu\in\mathbf{D} \tag{10}$$

The parameter-dependent energy inner product (11) and induced norm (12) are defined as [16], [31], [33]:

$$(((w,v)))_\mu = a(w,v;\mu) \qquad \forall w,v\in X \tag{11}$$

$$|||w|||_\mu = \sqrt{a(w,w;\mu)} \qquad \forall w\in X \tag{12}$$

Accordingly, we define the parameter-independent $X$-inner product (13) and induced norm (14) for a fixed $\mu$ (indicated by $\overline{\mu}$) as [16], [31], [33]:

$$(w,v)_X = (((w,v)))_{\overline{\mu}} \qquad \forall w,v\in X \tag{13}$$

$$\|w\|_X = \sqrt{(w,w)_X} \qquad \forall w\in X \tag{14}$$

The principal idea of the RB approach is to take advantage of the decomposition (3) – (5) by implementing an offline-online procedure. During the offline stage, all the expensive pre-computations are performed. The cost of these pre-computations is dependent on the high-dimensional FE solution because several solves of the full FE problem are required to build the low-order approximations, which will be explained in the following. Hence, it is advisable to perform the offline stage for large-scale models, where the solve of a single FE problem is already extremely time-consuming, on HPC infrastructures if available.

To construct the low-order approximations, we choose a parameter set $S_N = \{\mu^n, n = 1,...,N\}$ with snapshots $u^n = u(\mu^n)$ (Fig. 1) and define the RB approximation space $X_N = \mathrm{span}\{\mathrm{u}(\mu^\mathrm{n}), 1 \le \mathrm{n} \le \mathrm{N}\}$. Consequently, we define the

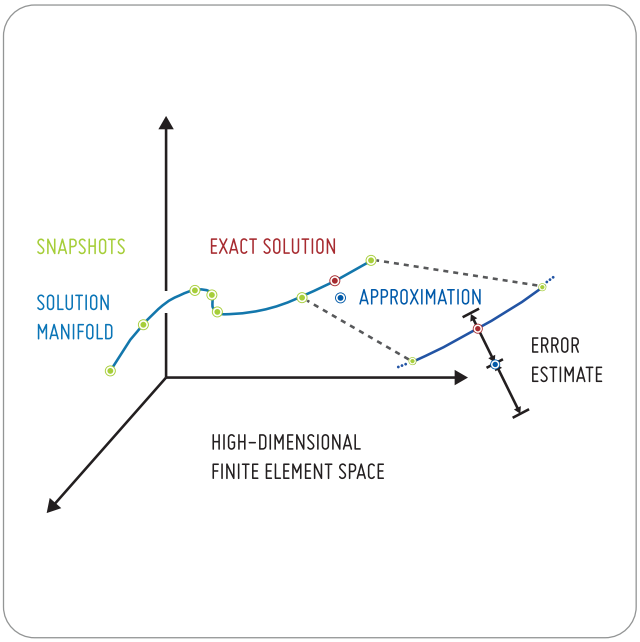


**Fig. 1** Schematic representation of the RB method. The snapshots are denoted in green, the exact solution in red, the approximation in blue and the space and error bound in black. Note, that the error bound is an approximation to the truth error. The error bound is for our examples large than the truth error.

Galerkin projection problem as follows, where $u_N \in X_N$ satisfies (15) [16], [31], [33]:

$$a(u_N(\mu),v;\mu) = f(v;\mu), \qquad \forall v\in X_N. \tag{15}$$

Afterwards, we evaluate (16)

$$s_N(\mu) = l(u_N(\mu);\mu). \tag{16}$$

The interesting question is how to retrieve and combine the snapshots in a meaningful way such that the obtained RB space is a good possible representation of the full FE space. For this reason, we introduce the error bounds in the following. We first have to define a coercivity constant lower bound of our problem as [16], [31], [33]. We employ the min-theta method [16] and define:

$$\alpha_{LB}(\mu) \equiv \theta_a^{\min,\overline{\mu}}(\mu) = \min_{q\in\{1,\dots,Q_a\}}\frac{\theta_a^q(\mu)}{\theta_a^q(\overline{\mu})}. \tag{17}$$

The min-theta method means that our coercivity constant is equal to the minimum parameter value, in our geothermal example it is consequently the lowest thermal conductivity.

We now define the residual and the associated Riesz representant [16], [31], [33]:

$$r(v;\mu) = f(v;\mu) - a(u_N(\mu),v;\mu), \tag{18}$$

$$(\hat{e}(\mu),v) = r(v;\mu). \tag{19}$$

The energy error bound (20) and the effectivity (21) are then [16], [31], [33]:

$$\Delta_N^{\text{en}}(\mu) \equiv \frac{\|\hat{e}(\mu)\|_X}{\alpha_{LB}^{\frac{1}{2}}(\mu)}, \quad (20) \qquad \eta_N^{\text{en}}(\mu) \equiv \frac{\Delta_N^{en}(\mu)}{|||\hat{e}(\mu)|||_\mu}. \quad (21)$$

Accordingly, the error bound (22) and effectivity (23) for the output are defined, respectively, as [16], [31], [33]:

$$\Delta_N^{\text{s}}(\mu) \equiv \frac{\|\hat{e}(\mu)\|_X^2}{\alpha_{LB}(\mu)}, \quad (22) \qquad \eta_N^{\text{s}}(\mu) \equiv \frac{\Delta_N^{s}(\mu)}{s(\mu) - s_N(\mu)}, \quad (23)$$

and those for the relative output error bound (25) is [16], [31], [33]:

$$\Delta_N^{\text{s,rel}}(\mu) \equiv \frac{\|\hat{e}(\mu)\|_X^2}{\alpha_{LB}(\mu) s_N(\mu)}, \qquad (24)$$

$$\eta_N^{\text{s,rel}}(\mu) \equiv \frac{\Delta_N^{\text{s,rel}}(\mu)}{\frac{s(\mu)-s_N(\mu)}{s(\mu)}}, \qquad (25)$$

In this paper we use the relative output error bound within the Greedy algorithm, explained below.

In space, the RB method uses a Greedy algorithm to construct the reduced basis. Performing the Greedy algorithm involves the following steps [40]:

Given, $\mu_1 \in \mathbf{D}$, $\mathrm{N} = 1$, $\varepsilon_{\text{tol,min}}$, $\Xi_{\text{train}} \in \mathbf{D}$
while $\Delta_N^{\max} \geq \varepsilon_{\text{tol,min}}$
  $N = N + 1$;
  $\mu_N^* = \arg \max_{\mu \in \Xi_{\text{train}}} \Delta_{N-1}(\mu)$;
  $S_N = S_{N-1} \cup \mu_N^*$;
  $X_N = X_{N-1} + \text{span}\{u^{\mathcal{N}}(\mu_N^*)\}$;
end

In essence, while the error is above a certain tolerance, the Greedy algorithm adds a new basis function by determining the member of the training set $\Xi_{train}$ at which the error bound is largest. This new parameter $\mu_N^*$ is then added to the sample $S_N$ and the normalized basis function $u(\mu_N^*)$ is added to the space of basis functions, $X_N$. This procedure is repeated until the chosen error tolerance is reached. In general, the error tolerance can be user-defined; in a geoscientific context, the tolerance can thus be adjusted according to, for instance, the measurement error. The benefits of this aspect are illustrated in Section 5.

In the offline-stage, performed once, we solve for the RB functions and hence the computational cost depends on the finite element space dimension $\mathcal{N}$. In the online-stage, performed many times - for each new $\mu$, the computational cost is of the dimension $N$. Considering $N \ll \mathcal{N}$, this means that the online stage has a much lower computational cost because of the largely reduced dimensionality of the problem [16], [31], [33], [39]. In case of our geothermal conduction example, we can perform the online-stage for any new thermal conductivity that falls within $\mathbf{D}$.

## 3 Methods and Models

As mentioned in Section 1, we implemented the RB method based upon the rbOOmit package within the MOOSE Framework. In the following, we will briefly discuss the advantages of the MOOSE framework for our application field. Throughout the entire paper, we consider a geothermal conduction problem and two different synthetic models, and one real-case model for demonstrating the general procedure of the RB method.

### 3.1 MOOSE Framework

The MOOSE Framework is in contrast to some other FE solvers, fully-coupled and has fully-implicit solvers. FE solvers are highly advantageous for geological studies since they allow discrete fracture analyses, as will be demonstrated by the second synthetic model. Additionally, MOOSE is built-up on top of the PETSc library, allowing an easy interfacing to advanced preconditioner settings. In the case of the RB method, it was furthermore beneficial that MOOSE is also based on the libMesh library since libMesh already has a package implementing the RB method. Our work within the software environment has been so far focused on integrating the existing libMesh package into the MOOSE Framework. This work has been realized within our MOOSE application named DwarfElephant. Using the MOOSE environment in addition to the libMesh library provides the user with several advantages such as a highly simplified model setup, an easier interchange of different physics, and simplified mesh modification. MOOSE uses a dimension independent physics; together with the object-oriented structure of the software, this allows an uncomplicated reuse and extensibility of pre-existing code structures. Another advantage of MOOSE is the built-in parallelization, meaning the same code can be used on desktop computers and on HPC infrastructures [36].

### 3.2 DwarfElephant

The DwarfElephant package is based on the MOOSE framework and aims at offering an user-friendly access to the reduced basis method. It is an open-source high-performance library written in the compute language C++. We based it on the libMesh implementation of the reduced basis method. Using the libMesh implementation directly, and not via the

MOOSE framework, has several disadvantages for geoscientific problems. Within the geoscientific community, we have to deal with rapidly changing geological models. Using the RB package within libMesh, this means that the entire working routine must be constructed again for each new model, which is an unnecessarily time-consuming task. The DwarfElephant package instead takes full advantage of the MOOSE capabilities. This allows an easy and fast interchange of different models due to several automated processes. It is furthermore possible to automatically apply different physics to different subdomains of the model because MOOSE operates on the individual subdomains separately. We take advantage of that by automatically separating the stiffness matrix with respect to the subdomains, but allowing also every other decomposition. This automatic separation provides an easier and faster way to simulate new models with the RB method. The load vector is not automatically separated, since this is often not required, but as for the stiffness matrix any kind of decomposition can be done. We developed the software on purpose in a physics-independent framework in order to allow an usability of the software also outside of the geoscientific community. The DwarfElephant package is furthermore easily compatible with other MOOSE application, such as GOLEM [18] and REDBACK [30].

### 3.3 Geothermal Conduction

In the following we consider a geothermal conduction problem as given in (26) as a motivating geoscientific example:

$$\lambda \nabla^2 T = 0 \qquad \text{in } \Omega, \tag{26}$$

where $\lambda$ is the thermal conductivity and $T$ the temperature. In our case, we consider a steady-state problem without sources and sinks, thus ending up with an elliptic PDE. A Dirichlet boundary condition is applied at the top of the domain, whereas a Neumann boundary condition is used at the bottom.

For performance and convergence reasons we take only dimensionless parameters and variables into account. Therefore, we non-dimensionalize the length by (27):

$$l^* = \frac{l}{l_{\text{ref}}}. \tag{27}$$

Throughout the entire paper, the stars or asterisks denote the dimensionless quantities; the quantities without any asterisks refer to the dimensional quantities and the "ref" denotes the reference parameter used for the non-dimensionalization.

The thermal conductivity is non-dimensionalized by applying (28):

$$\lambda^* = \frac{\lambda}{\lambda_{\text{ref}}}. \tag{28}$$

Finally, the non-dimensionalization of the temperature is performed with (29):

$$T^* = \frac{T - T_{\text{ref}}}{T_{\text{ref}}}. \tag{29}$$

### 3.4 Models

In this paper, we consider two different synthetic models. For performance issues we consider dimensionless meshes with an extension in $x$-, $y$-, and $z$-direction from 0 to 1. The reference length is 1,000 m, the reference thermal conductivity 1.05 W $m^{-1}$ $K^{-1}$ (i.e, the smallest thermal conductivity), and the reference temperature 10 °C. The first model consists of three parallel layers (further referred to as the "Base model"), and the second has the same three layers and additionally two faults (the "Fault model"). The younger fault offsets the layers by 0.06 (corresponding to 60 m) and the older fault by 0.05 (50 m). The layer offset produced by the older fault is 0.02 (20 m). Figure 2 displays a schematic representation of the two different models. In both cases, the top and bottom layer are shale layers, whereas the middle layer consists of a more conductive sandstone. For all rock types typical thermal conductivities (see Table 1) are assumed [27]. The faults, only present in the second model, have the same thermal conductivities, which are the highest thermal conductivities within the entire model. The faults have a dip of 45°. Note that the thermal conductivity is also taken as a non-dimensional parameter.

For the meshing, we used the MeshIT software developed by the Geoforschungszentrum Potsdam [6] and Gmsh [11]. Both models have tetrahedron meshes. Furthermore, the faults are considered as discrete 2D elements in the 3D mesh, and are constructed through triangular elements. Table 2 lists the different meshes and their properties. For the Base model, the degrees of freedom are varying from 1,426 to 1,512,161. All meshes have the same geometries and only differ in their global refinement level. Note that for each global refinement factor a new mesh has been created. We did not refine the pre-existing mesh in order to prevent error by refining possible ill-created mesh elements. The meshes of the Fault model, varying from 4,600 degrees of freedom to 1,969,077, are generated in the same way as for the Base model but using the meshing software Gmsh instead of MeshIT in order to demonstrate the usability of different meshing software within the package. The faults are always considered with a global refinement that is twice as fine as the layers. All simulation-relevant parameters can be found

in Tab. 3 for the FE and RB method. Note that for the RB method the same parameters have been chosen as for the FE method. Hence, they are not listed again in the RB section of Tab. 3. In this section, parameters additionally required for the RB method are mentioned only. The larger meshes of the Fault model required a higher solver tolerance in order to avoid rounding errors during the Greedy algorithm. We thus made another set of simulations with smaller solver tolerances of $10^{-9}$ for the RB and FE model.

Both models have a Dirichlet boundary condition of 10 °C at the top and a Neumann boundary condition of 0.039 W $m^{-2}$ at the bottom. The Neumann condition represents a normal geothermal gradient with a temperature increase of about 30 °C per kilometer. At the top, the average annual temperature is used as a Dirichlet boundary condition. Correspondingly, the dimensionless top boundary condition is 0 and the bottom boundary condition is 3.71 (choosing a standard basin heat flux). Note, for the RB method we have considered three parameters in case of the Base model, and five parameters in case of the Fault model. That means although we made our simulations with equal thermal conductivities for layer 1 and 3 and equal thermal conductivities for both faults we have the flexibility to set them to non-equal values.

Furthermore, we consider as a real-case large-scale geological model the Perth Basin (Australia) modified after [43] and displayed in Fig. 3. We use a reference length of 70,000 m, a reference thermal conductivity of 4.3 W $m^{-1}$ $K^{-1}$ (i.e, the largest thermal conductivity), and a reference temperature of 22 °C. It has a spatial extension of 0.90 (63 km) in x-direction, 1.00 (70 km) in y-direction and 0.27 (19 km) in z-direction. It consists of six layers and is displayed in Figure 3. We vary the thermal conductivities in all six layers. At the top of the model, a Dirichlet boundary condition with a value of 0 (22 °C) is applied, corresponding to the annual average temperature of Australia. For the bottom boundary condition, we use a Neumann boundary condition with a value of 19.24 (0.026 W $m^{-2}$), which is the average basin heat flux of the Perth Basin. All thermal properties can be found in Table 1 and all simulation properties in Table 3. The model itself was generated using GemPy [38] and meshed using the "GeneratedMesh" functionality of MOOSE, resulting in a hexahedral mesh with 1,771,561 degrees of freedom.

We performed all simulations on the RWTH compute cluster on an Intel Westmere X5675 (3.07 GHz, 6 cores per chip, 12 cores per node and 24 GB memory per node) using one CPU core. Only the performance tests (see Section 5) have been simulated using Intel Xeon E5-2680 v3 Haswell nodes on the JURECA compute cluster (2.5 GHz, 24 cores per node and 128 GB memory per node) [20].

In order to achieve convergence for the larger models, a preconditioner is required. We chose the hypre preconditioner of the type boomerang. This PETSc preconditioner is a matrix element based preconditioner that can be found in the LLNL package hypre [3]. Additionally, one should note that MOOSE is a state-of-the-art forward solver. Thus, we have a highly efficient FE solve, which effects the speed-up (shown in Section 4) since the preconditioning does not influence the online times because of the dense nature.

We now apply the RB approach to geothermal conduction simulations in different scenarios to evaluate the speed-up.

## 4 Results

The biggest advantage in case of the RB method is certainly the speed-up. Therefore, Fig. 4 compares the runtime of the FE and RB simulations and additionally plots the speed-ups obtained by the RB approach. First of all, we can see that we get a significant speed-up with a maximum value of 1,009.5 for the Base model with 1,512,161 degrees of freedom but maybe even more important is to note that this speed-up is higher for the larger models. Hence, we observe a speed-up variation from 33.4 to 1,009.5 for an increase in the degrees of freedom from 1,426 to 1,512,161.

For the Fault model, we observe speed-ups between 32.0 and 1,138.5 for solver tolerances of $10^{-9}$. We get smaller speed-ups for the Fault model than for the Base for similar model sizes. The reasons for this are illustrated in Section 5.

The FE solution of the Perth Basin model requires 160.24 s, whereas the RB solution takes only 0.21 s. Hence, the speed-up of the Perth Basin model is 752.3 for a solver tolerance of $10^{-8}$.

After showing how much faster simulations can be performed with the RB method, we have to validate that the results for the method are qualitatively and quantitatively comparable to the FE solutions. Therefore, we simulated both models, with the properties given in the previous section, taking the standard finite element and the reduced basis method into account.

Figure 5 shows the simulation results for the Base and the Fault model under consideration of the RB method. Note that Figure 5 shows only the results of the RB method. The results of the FE method are not plotted since they are not distinguishable in the temperature plot due to the very small errors of the RB method (see Figure 7). In Fig. 5a we observe the expected temperature diffusion for a three-layer scenario with a more conductive middle layer. So, the top and bottom layer have the highest temperature increase of 1.26 (12.6 °C) and 1.22 (12.2 °C), respectively. This is due to the lower thermal conductivity. In contrast, the middle layer has a lower temperature increase of 0.52 (5.2 °C) because of the higher thermal conductivity. For the Base model, we encounter parallel temperature isolines following the geological layers and varying from a minimum temperature of

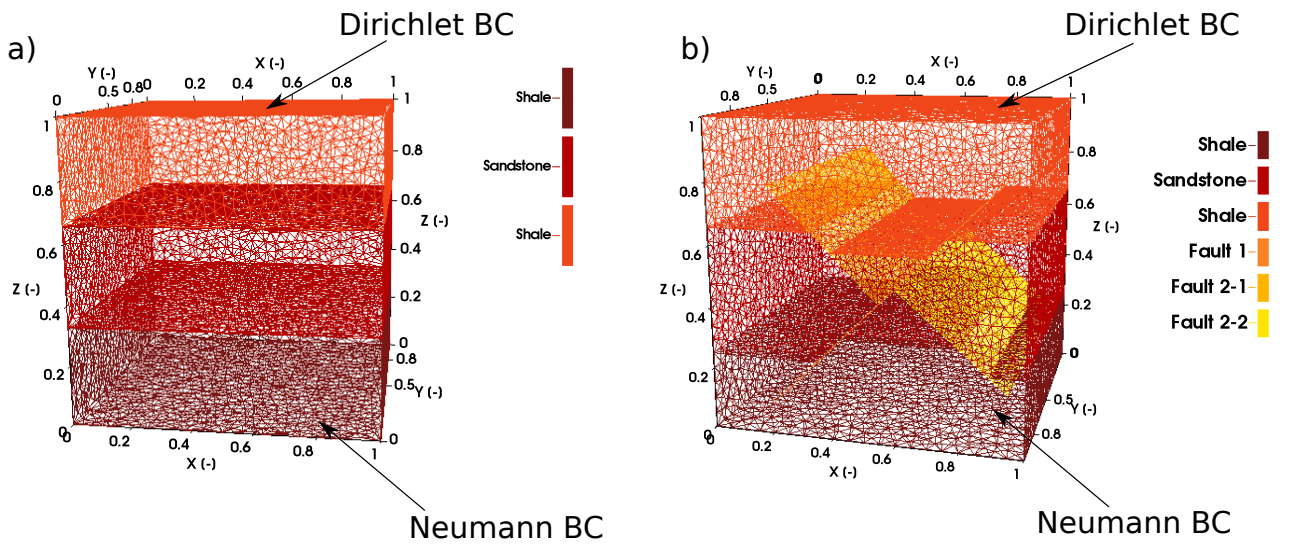


**Fig. 2** Mesh representation of a) the Base model consisting of three parallel layers (11, 269 degrees of freedom) and b) the Fault model consisting of three layers and two faults (23,860 degrees of freedom). Both models have a Dirichlet boundary condition at the top and a Neumann boundary condition at the bottom of the respective model. Note that the mesh is dimensionless for performance issues.

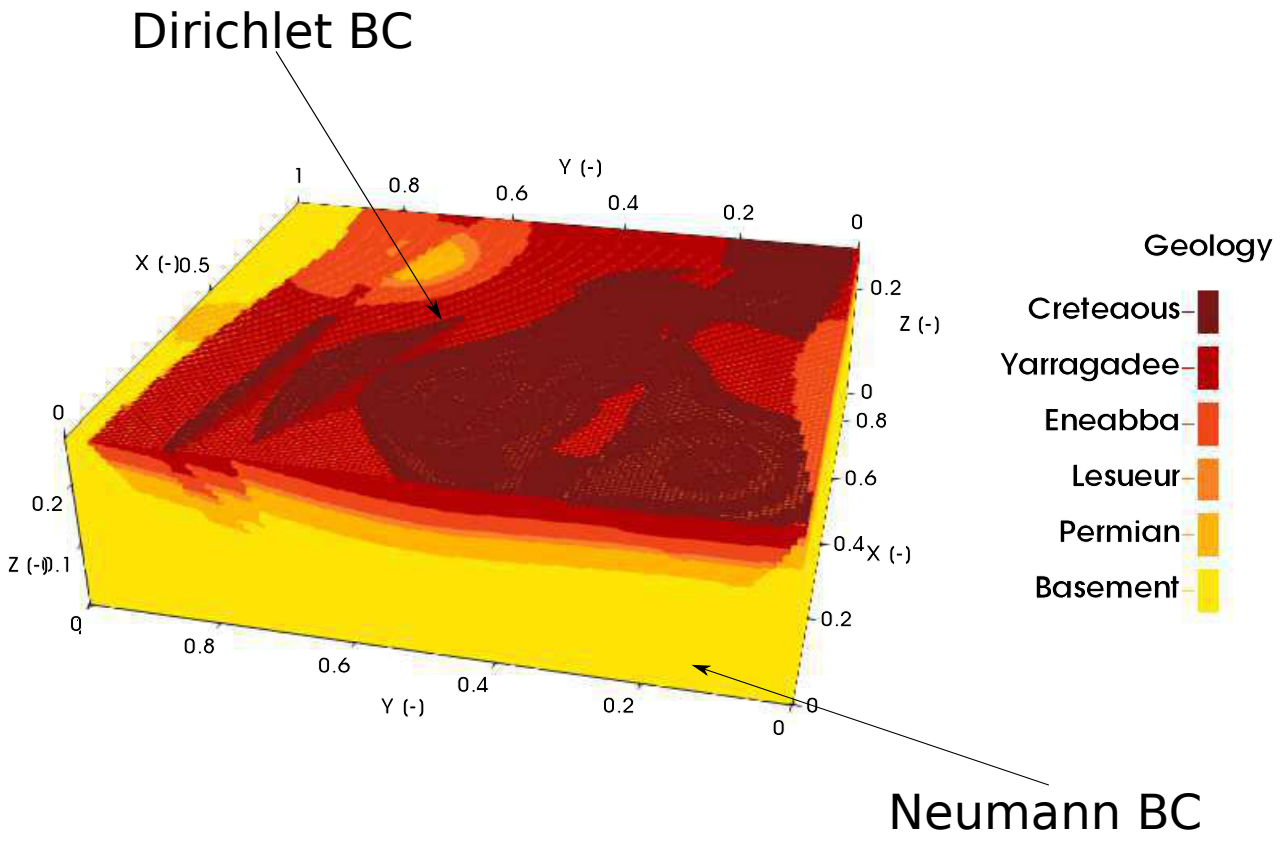


**Fig. 3** Mesh representation of the Perth Basin model with 1,771,561 degrees of freedom. The model has a Dirichlet boundary condition at the top and a Neumann boundary condition at the bottom of the respective model. Note that the mesh is dimensionless for performance issues.

**Table 1** Thermal and model properties for both the synthetic models [27] and the Perth Basin [43]. Take into account that both the thermal conductivity and the length are dimensionless.

| unit | thermal conductivity [W $m^{-1}$ $K^{-1}$] / thermal conductivity [-] | extension in x-direction [-] | extension in y-direction [-] | extension in z-direction [-] |
|---|---|---|---|---|
| **Base model** | | | | |
| top layer (shale) | 1.05 / 1.00 | 0.00 - 1.00 | 0.00 - 1.00 | 0.66 - 1.00 |
| middle layer (sandstone) | 2.50 / 2.38 | 0.00 - 1.00 | 0.00 - 1.00 | 0.33 - 0.66 |
| bottom layer (shale) | 1.05 / 1.0 | 0.00 - 1.00 | 0.00 - 1.00 | 0.00 - 0.33 |
| **Fault model** | | | | |
| top layer - section 1 (shale) | 1.05 / 1.00 | 0.00 - 0.34 | 0.00 - 1.00 | 0.66 - 1.00 |
| top layer - section 2 (shale) | 1.05 / 1.00 | 0.40 - 0.70 | 0.00 - 1.00 | 0.60 - 1.00 |
| top layer - section 3 (shale) | 1.05 / 1.00 | 0.76 - 1.00 | 0.00 - 1.00 | 0.66 - 1.00 |
| middle layer - section 1 (sandstone) | 2.50 / 2.38 | 0.00 - 0.34 | 0.00 - 1.00 | 0.25 - 0.66 |
| middle layer - section 2 (sandstone) | 2.50 / 2.38 | 0.43 - 0.70 | 0.00 - 1.00 | 0.33 - 0.60 |
| middle layer - section 3 (sandstone) | 2.50 / 2.38 | 0.89 - 1.00 | 0.00 - 1.00 | 0.25 - 0.66 |
| bottom layer - section 1 (shale) | 1.05 / 1.00 | 0.00 - 0.35 | 0.00 - 1.00 | 0.00 - 0.25 |
| bottom layer - section 2 (shale) | 1.05 / 1.00 | 0.43 - 0.80 | 0.00 - 1.00 | 0.00 - 0.33 |
| bottom layer - section 3 (shale) | 1.05 / 1.00 | 0.89 - 1.00 | 0.00 - 1.00 | 0.00 - 0.25 |
| Fault 2 | 3.00 / 2.86 | 0.20 - 0.90 | 0.00 - 1.00 | 0.10 - 0.80 |
| Fault 1 - section 1 | 3.00 / 2.86 | 0.20 - 0.55 | 0.00 - 1.00 | 0.45 - 0.80 |
| Fault 1 - section 2 | 3.00 / 2.86 | 0.60 - 0.95 | 0.00 - 1.00 | 0.20 - 0.50 |
| **Perth Basin model** | | | | |
| Cretaceous | 3.9 / 0.91 | - | - | - |
| Yarragadee | 4.3 / 1.00 | - | - | - |
| Eneabba | 3.85 / 0.90 | - | - | - |
| Lesueur | 3.8 / 0.88 | - | - | - |
| Permian | 3.1 / 0.72 | - | - | - |
| Basement | 2.7 /0.63 | - | - | - |

**Table 2** Mesh properties for both the synthetic models and the Perth Basin.

| model | refinement layer | refinement fault | # elements | # nodes |
|---|---|---|---|---|
| Base model | 0.12 | - | 6,351 | 1,426 |
| | 0.1 | - | 10,975 | 2,378 |
| | 0.05 | - | 56,222 | 11,269 |
| | 0.04 | - | 94,749 | 18,692 |
| | 0.03 | - | 179,976 | 34,989 |
| | 0.02 | - | 437,183 | 83,924 |
| | 0.015 | - | 808,468 | 154,181 |
| | 0.01 | - | 1,908,931 | 361,967 |
| | 0.009 | - | 2,374,382 | 449,662 |
| | 0.008 | - | 3,035,457 | 574,241 |
| | 0.007 | - | 4,004,907 | 756,814 |
| | 0.006 | - | 5,510,748 | 1,040,333 |
| | 0.005 | - | 8,021,256 | 1,512,161 |
| Fault model | 0.1 | 0.05 | 26,742 | 4,600 |
| | 0.05 | 0.025 | 1142,576 | 23,860 |
| | 0.025 | 0.0125 | 896,885 | 149,490 |
| | 0.0125 | 0.00625 | 6,235,267 | 1,040,325 |
| | 0.01 | 0.005 | 11,796,240 | 1,969,077 |
| Perth Basin model | - | - | 1,728,000 | 1,771,561 |

**Table 3** Simulation parameters for the finite element and the reduced basis method of both synthetic models and the Perth Basin.

| Simulation parameter | Value | | |
|---|---|---|---|
| | Base model | Fault model | Perth Basin model |
| **FE method** | | | |
| Solver type | | Newton | |
| Linear solver tolerance | $10^{-8}$ | $10^{-8}$/$10^{-9}$ | $10^{-8}$ |
| Nonlinear solver tolerance | $10^{-8}$ | $10^{-8}$/$10^{-9}$ | $10^{-8}$ |
| Preconditioner type | | hypre | |
| Hypre type | | boomerang | |
| ksp_gmres_restart | | 101 | |
| **RB method** | | | |
| Rel. training tolerance | | $10^{-5}$ | $10^{-3}$ |
| Parameter ranges (Layer 1) | | 0.5 to 5.0 | 0.453 to 1.360 |
| Parameter range (Layer 2) | | 0.5 to 7.0 | 0.500 to 1.500 |
| Parameter range (Layer 3) | | 0.5 to 5.0 | 0.448 to 1.343 |
| Parameter range (Layer 4) | | 0.5 to 5.0 | 0.441 to 1.325 |
| Parameter range (Layer 5) | | 0.5 to 5.0 | 0.360 to 1.081 |
| Parameter range (Layer 6) | | 0.5 to 5.0 | 0.313 to 0.941 |
| Parameter ranges (Faults) | - | 0.5 to 4.0 | - |
| Number of parameters | 3 | 5 | 6 |
| Number of training sample | 5 | 100 | 100 |
| Maximum number of basis function | 5 | 100 | 50 |

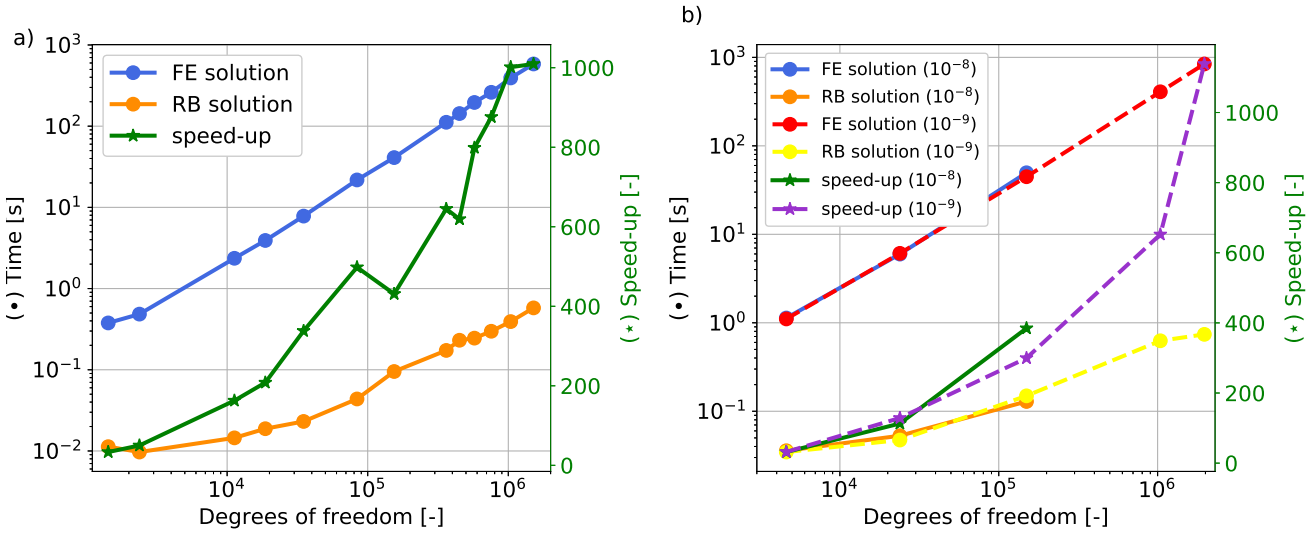


**Fig. 4** Runtime comparison between the full finite element solution –denoted in blue– and the RB solution –denoted in orange– for the a) Base model and b) Fault model with permeable faults with a solver tolerance of $10^{-8}$. Additionally, in b) the red dashed line denotes the FE solution and the yellow dashed line the RB solution for a tolerance of $10^{-9}$. Furthermore, the blue line illustrates the speed-up with a solver tolerance of $10^{-8}$ and the violet dashed line the speed-up with a solver tolerance of $10^{-9}$.

0.0 (corresponding to 10.0 °C) and a maximum temperature of 3.0 (corresponding to 40.0 °C).

The image slightly changes for the Fault model (Fig. 5b). Here, we consider permeable faults (Fig. 5b). In case of the permeable faults, the highly conductive faults yield a lower maximum temperature of 2.22 (32.2 °C) and curved temperature isolines following both fault structures. We thus observe an x-like structure for the isolines around the faults. These results are in accordance with our expectations since the heat transport prefers higher over lower conductive zones. This means that in case of high conductive faults, the faults will be the preferential path for the heat transport as seen in Fig. 5b.

The temperature distribution (Fig. 6) of the Perth Basin resembles the one from the Base model, with the differences that the isolines are slightly curved towards the center of the basin. The temperature gradient has its minimal non-dimensionalized value of 0.0 (corresponds to 22.0 °C) at the

top of the model and its maximum value of 7.7 (corresponds to 191,4 °C in the dimensionalized model) at the bottom of the model. Note that we are again only plotting the results of the reduced basis solution since due to the small errors (Fig. 8), no differences are visible in this representation.

After validating that we are able to qualitatively reproduce the FE solutions with the RB method, we want to illustrate the quantitative differences between both methods. As with any kind of approximation, we face the question of the price we have to pay for our speed-up. Usually, we pay by losing accuracy; the important aspect is naturally how high this accuracy loss will be. For this purpose, we performed the same simulation with the same conditions and within the same software with *i)* the finite element method and *ii)* the reduced basis method. Afterwards, we generated a difference plot between both simulations (Fig. 7). For both synthetic models we reach our given relative error tolerance of $10^{-5}$ and for the Perth Basin we reach the tolerance of $10^{-3}$. We have a different error tolerance for the Perth Basin in order to demonstrate how this parameter is adjustable to measurement data. The tolerance is choosen such that the obtained simulations are more accurate than the measurements to ensure that no additional errors are introduced by the reduction itself. For all models, we observe the largest errors at the layer interfaces, caused by the abrupt change of the parameter value.

Additionally, we present a plot of the reduced basis convergence rate in Fig. 9. In this figure, the maximum error bound is plotted as a function of the number of basis functions. We considered again the Base and Fault model for varying numbers of degrees of freedom. In the case of the Base model the observations are two-fold: First, we generally have lower error bounds for smaller model sizes; and second, adding the first and second basis functions has a much smaller impact on the error bound than adding the third basis function. In case of the Fault model, we cannot observe generally higher error bounds for the larger models, instead, no specific pattern is observable. For the Fault model, we obtain a varying number of basis functions in order to reach our predefined tolerance. The variation is caused by the random selection of training parameters and not by the model size. As for the Base model, we see the same behavior in the convergence rate independent of the degrees of freedom. For the Perth Basin (Fig. 10) the maximum relative error decreases similarly to the Fault model. Also for this real-case model we reach the predefined error tolerance of $10^{-3}$.

In Fig. 11 we show the runtimes (including the offline phase) for both the FE and RB simulations considering several simulations. For these result, we only made one simulation and extrapolate the runtime for the other simulations. Thus, we do not account for performance fluctuations of the cluster.

It can be seen that for the Base model already two to seven simulations are enough for the RB method (with the cost of offline and online stages combined) to be more efficient than the FE method. For the Fault model, more basis functions are necessary; they vary between 58 and 62 (Fig. 12). Hence, the offline phase of the Fault model is more time-consuming than the one of the Base model since every new basis function requires an FE solve. Considering that the offline stage of the Perth Basin takes 12,719.78 s we need 80 simulations before the RB method is computationally more efficient than the FE method.

Figure 13 shows that for the Base model 1,426 degrees of freedom are already enough to reach convergence, whereas for the Fault model we reach convergence after 1,040,325 degrees of freedom. For the latter model, we need a much finer mesh because the simulation results are highly affected by the two faults. The degrees of freedom that are necessary to reach convergence could be reduced by, for instance, adaptive mesh refinement methods.

## 5 Discussion

The aim of this paper is to demonstrate that the computation time for a geothermal forward simulation can be drastically reduced without a major quality degradation by using the RB instead of the FE method. In this context, we observe in Fig. 4 an increase in the speed-up for both the Base and the Fault model with increasing degrees of freedom. An explanation to this is found by having a closer look at the dimensionality changes of the FE and RB space (Fig. 12). The dimension increase of the RB space is much smaller than that of the FE space due to the fact that although the dimension of the FE space has increased, the complexity of the parameter dependence for the two problems remains more or less the same. The different dimensionality can be seen in Fig. 12, where we see that in the RB method, three basis functions suffice to represent the parameter-dependence of the problem. The RB method thus has great potential for large scale models, which have an underlying low-dimensional parameter dependence, as demonstrated for the Perth Basin model. This might be especially beneficial for geoscientific applications, which are usually high-dimensional such as seismic applications [15], stochastic problems [8] and data assimilation problems [25]. In Fig. 4 we can also see that we do not always get an higher speed-up for more degrees of freedom. The problem is that the online time takes, depending on the model size, between 9.7 ms and 578.2 ms, because of these small runtimes fluctuations in the cluster performance due to different workloads have a significant influence. Thus, we always observe a speed-up but the increase in speed-up might be smaller than expected.

In order to explain the decreased speed-ups for the Fault model, we have to look at the runtimes for the FE simula-

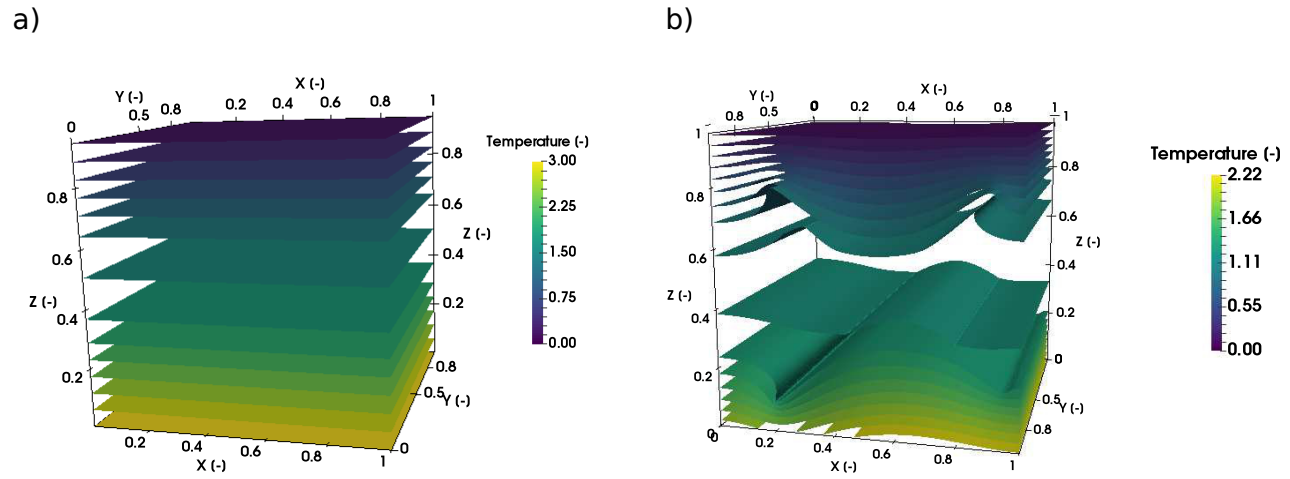


**Fig. 5** Temperature distribution for a) the Base model, b) Fault model with permeable faults. Note that the both the mesh dimensions, and the temperature have been normalized for numerical reasons, and are hence dimensionless. Both models have a reference temperature of 10 °C, a reference length of 1,000 m and solver tolerances of a) $10^{-8}$ and b) $10^{-9}$.

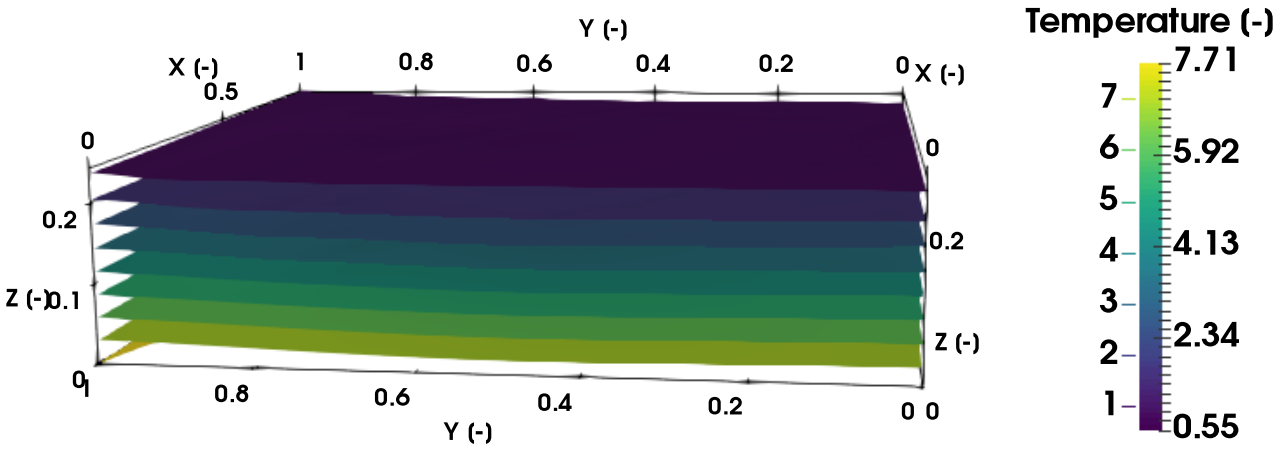


**Fig. 6** Temperature distribution for the Perth Basin model. Note that the both the mesh dimensions, and the temperature have been normalized for numerical reasons, and are hence dimensionless. The model has a reference temperature of 22 °C, a reference length of 70,000 m and solver tolerances of a) $10^{-8}$.

tions. If we take, for instance, the Base model with 2,378 degrees of freedom and the Fault model with 4,600 degrees of freedom we observe an increase in the runtime from 0.485 s to 1.106 s (an increase of 128 %). For the online times, we observe an increase from 0.097 s to 0.0346 s (257 %), which results in the smaller speed-up. The reason why the online time has increased by this amount is due to the increase in the number of basis functions from 3 to 62 (Fig. 12). Also, the Perth Basin shows a decreased speed-up in comparison to the Base model, which is induced by the higher complexity due to the variation of six instead of three parameters. Furthermore, note that we defined three parameters for the Base model and five parameters for the Fault model, although we consider equal thermal conductivities in layer 1 and 3 and in both faults. Thus, two parameters in the case of the Base model and three parameters in the Fault model would be sufficient to describe our problem. Using three instead of five parameters would lead to a reduced number of basis functions, which would yield a faster offline and online phase. As previously mentioned, we have chosen a higher number of parameters for obtaining a more flexible model.

In the case of the Base model, we reach an error tolerance that is far below our threshold due to the big error reduction introduced by the third basis function (Fig. 9). This is caused by the simplicity of the model. It consists of three

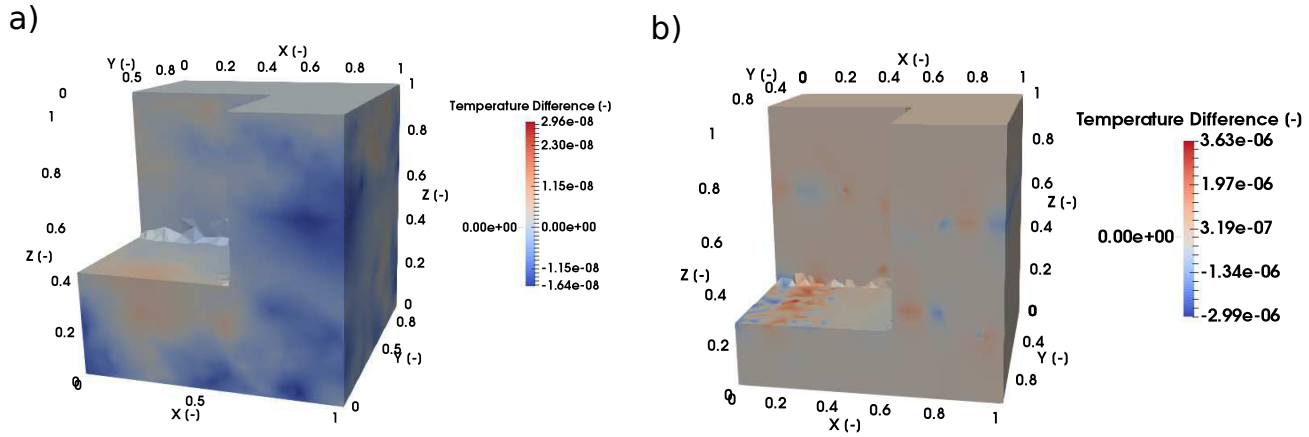


**Fig. 7** Difference plot between the full finite element and the reduced basis solution for the a) Base model, b) Fault model with permeable faults. The relative error tolerance was set for all cases to $10^{-5}$, and the solver tolerances to a) $10^{-8}$ and b) $10^{-9}$.

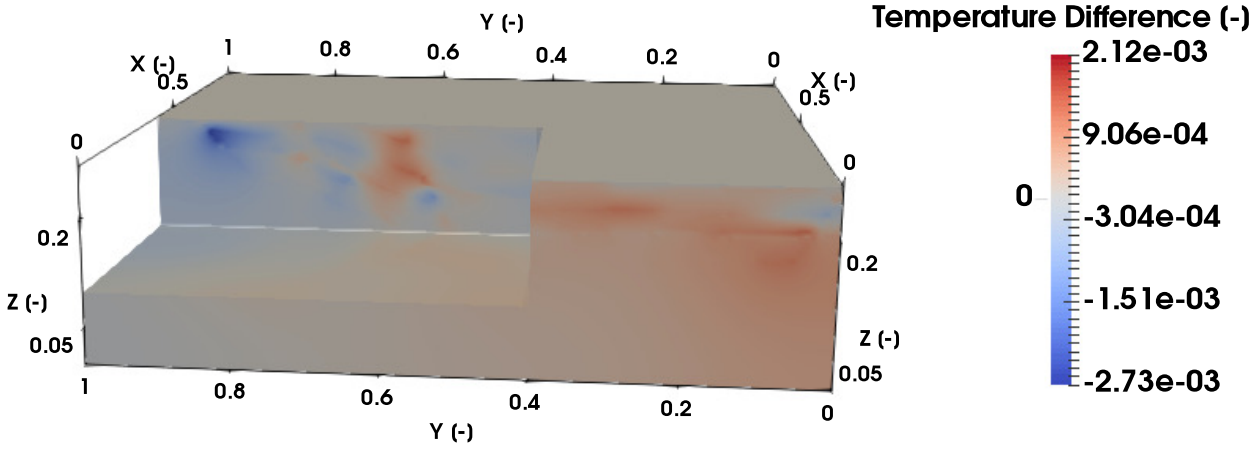


**Fig. 8** Difference plot between the full finite element and the reduced basis solution for the Perth Basin model. The relative error tolerance was set to $10^{-3}$, and the solver tolerances to $10^{-8}$.

layers with varying thermal conductivities. For this problem, we require three basis functions to capture the variability. More complex models would naturally require more basis functions. The reduction in the error is even larger than the defined tolerance for the third basis function since we can now fully describe the model, whereas for the first and second basis function crucial information is missing to fully describe the model. The Fault model does not show this behavior since it is more complex and the reduced model does not yet fully capture the entire complexity. The accuracy loss is therefore far below the typical measurement error of a geothermal temperature measurement, i.e., we do not introduce additional error sources through the RB method. In this paper, we have chosen a lower tolerance value than necessary in order to demonstrate the precision of the RB method. If desired, even more, precise results can be obtained by further lowering the tolerance. However, it should be taken into account that a higher precision results in a higher number of basis functions which in turn decreases the speed-up and increases the time required for the basis construction. For normal temperature simulations, a relative tolerance of $10^{-3}$ is sufficient. With this tolerance, we guarantee that the introduced error through the approximation is below our measurement error. In case of the Perth Basin model we already demonstrated how the tolerance is adjustable to the measurement error, and for this reason we have chosen in the real-case example a more realistic tolerance.

We observed generally increasing error bounds with increasing model sizes for the Base and Fault model. This indicates that if we would continue increasing our model size we would, at some point, require additional basis functions in order to obtain a good representation of the FE space. Furthermore, it should be taken into account that the general trends in the convergence rate do not change for different model sizes.

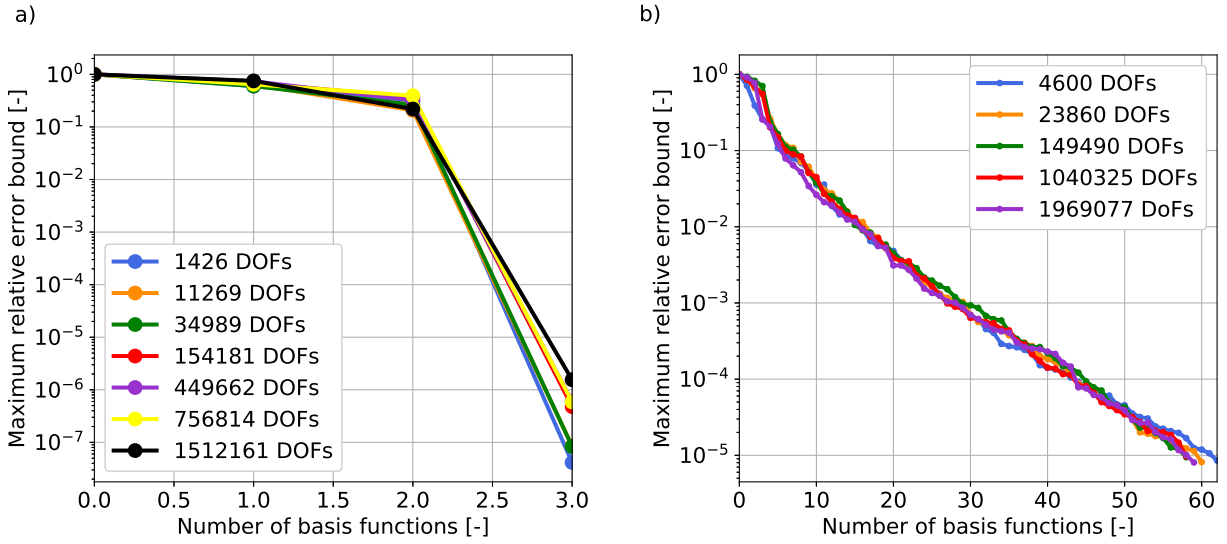


**Fig. 9** Convergence rate of the construction of the RB space for the a) Base model and b) Fault model for varying degrees of freedom and a relative error tolerance of $10^{-5}$ and solver tolerances of a) $10^{-8}$ and b) $10^{-9}$.

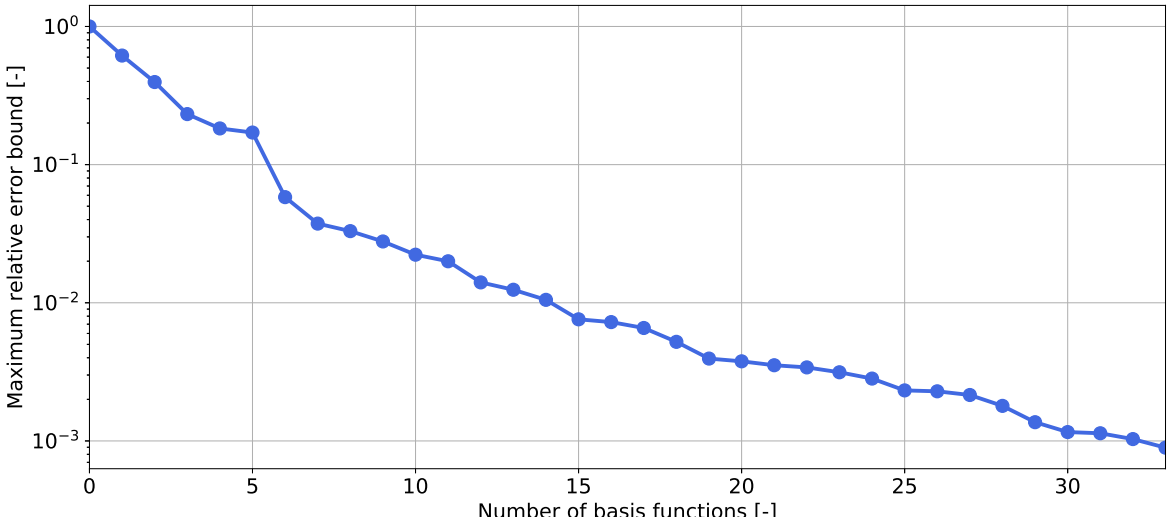


**Fig. 10** Convergence rate of the construction of the RB space for the Perth Basin model for a relative error tolerance of $10^{-3}$ and solver tolerances of $10^{-8}$.

A major shortcoming of the RB method is the expensive and time-consuming offline phase, where the construction of the reduced basis takes place. Although it is time-consuming, it only has to be performed once. For that reason, the method is more efficient than the FE method when we require numerous simulations as shown in Fig. 11. Although we did not account for performance fluctuations of the cluster, we get a realistic representation of the simulations required for the RB method to be beneficial over the FE method because only the online time is greatly influenced by fluctuations. As mentioned previously the online times are extremely small, and therefore the fluctuation effects will be barely visible for these kinds of analyses. To further demonstrate this, we show during the performance test the same analysis performed with varying degrees of freedom simulated at different times and hence with different workloads of the cluster.

In Fig. 11 the intersection between the dashed lines (RB) and the solid lines (FE) denotes the number of simulations required for the RB method to be more efficient than the FE method. The position of the intersection is for both models not dependent on the degrees of freedom. For the Base model, it is caused by the mentioned fluctuations of the compute cluster. This is also one of the reasons for the variability

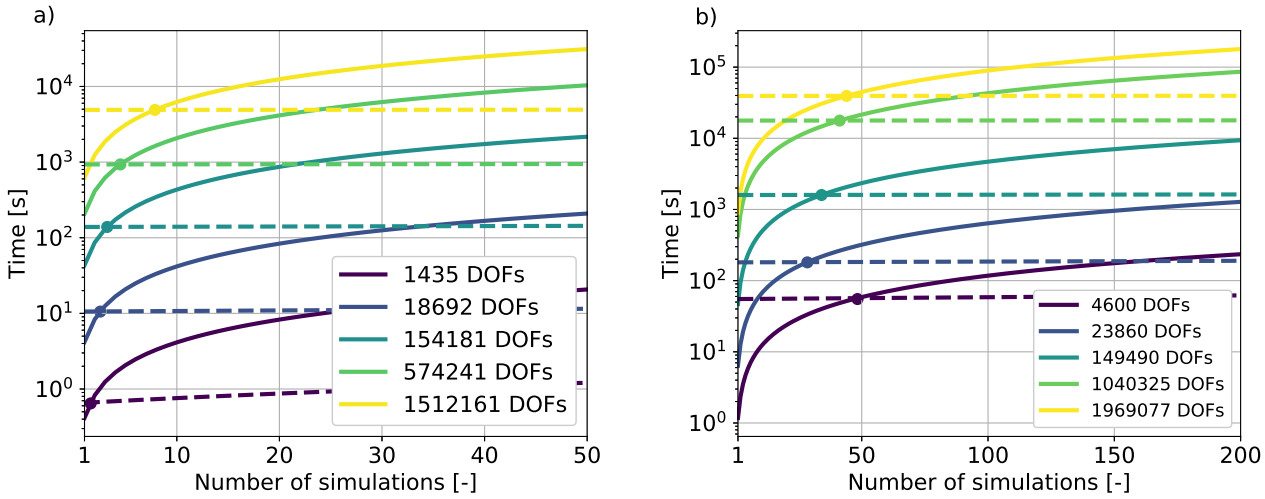


**Fig. 11** Comparison of the runtimes for the FE approach (solid lines) and the combined offline and online times of the RB approach (dashed lines) for varying degrees of freedom and solver tolerances of $10^{-8}$ for a) the Base model and b) the Fault model over 50 and 200 simulations, respectively.

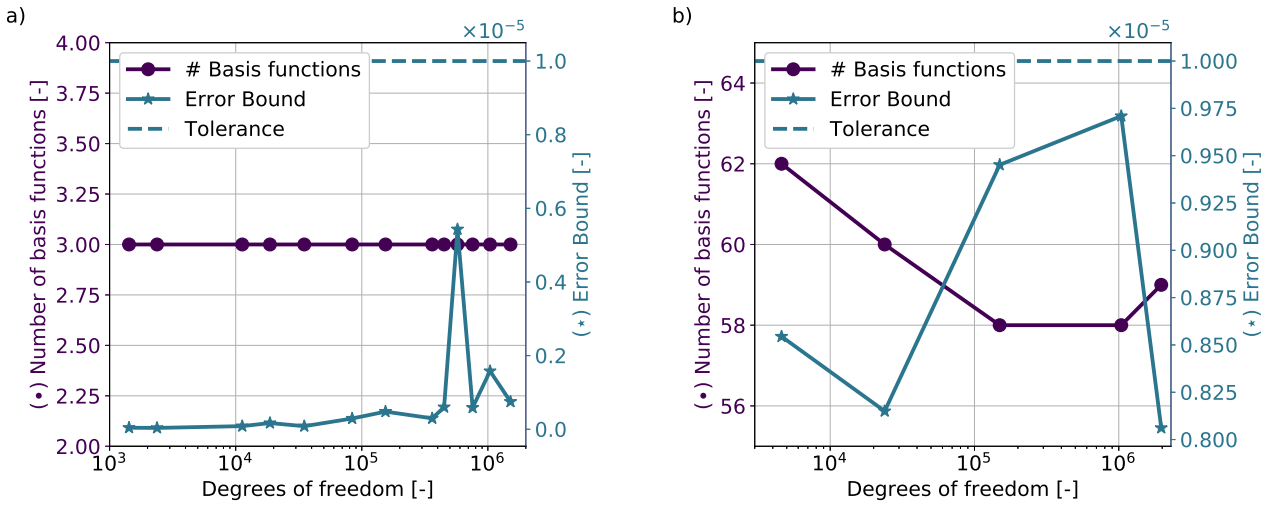


**Fig. 12** The evolution of the maximum error bound at the final basis function, and the number of basis functions required for reaching a relative tolerance of $10^{-5}$ by using solver tolerances of $10^{-8}$ for the a) Base model and b) Fault model.

of the intersection position for the Fault model. The other reason is that we chose our training parameters randomly. Hence, with a specifically tailored training set, the number of required basis functions for each realization would be lower. Due to the randomness, the difference to this optimal set varies for each of these realizations, and therefore the position of the intersection changes.

Regarding the Base model, three basis functions have been enough for describing the model. Due to the low number of basis functions, the construction of the basis is relatively fast, and therefore the RB method pays off rather quickly. Furthermore, the complexity of the offline phase depends on the dimension of the FE problem. The increase in the online time with increasing degrees of freedom is negligible in comparison to the FE runtimes. Accordingly, no relationship between the model size and the threshold at which the RB method is more efficient than the FE method is observable. Note that, as an example, for a model with 1,512,161 degrees of freedom, 50 FE simulations would require approximately 8 hours, whereas the same number of simulations using the RB method (including the offline time) are approximately six times faster. In case the offline stage

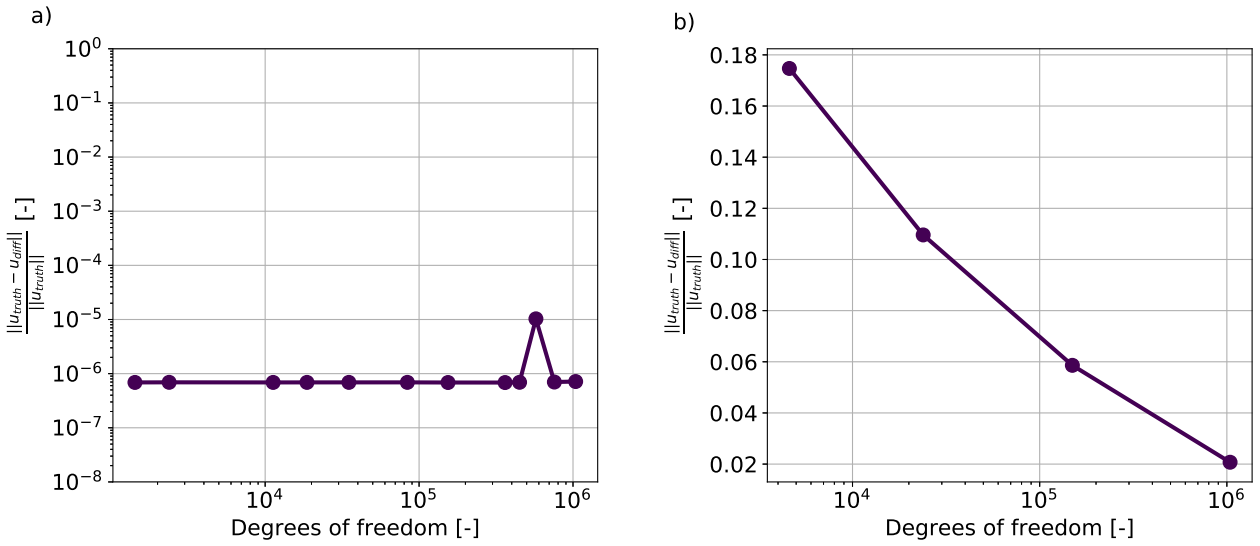


**Fig. 13** $H_0^1$ norm for the a) Base model and b) Fault model for varying degrees of freedom and a relative error tolerance of $10^{-5}$, and solver tolerances of $10^{-9}$.

has already been performed, the simulation would require approximately 0.1 % of the FE compute time.

The offline phase of the Fault model took more computation time than the one for the Base model, because more basis functions are required to represent the model. Consequently, it takes more simulation runs for the RB method to be more efficient than the FE method. In our example, we required between 29 and 48 simulations. Taking, for instance, 200 runs of the model with 1,969,077 degrees of freedom into account we would need nearly 50 hours with the FE approach and are 4.5 times faster with the RB method (including the offline time). The difference of the runtime between both methods would further increase with more simulations since most of the time for the RB method is spent during the offline phase, which has to be computed only once. The online stage for 200 simulations needs less than 0.1 % of the FE compute time. Furthermore, the number of basis functions is highly model-specific. If we take the Fault model and apply the boundary conditions to the left and right side of the model, we only need around 20 basis functions, which decreases the offline phase, and hence results in an earlier pay-off.

For the Perth Basin model, we require at least 80 simulations to be more efficient with the RB method than the FE method. If we take again the example of 200 simulations, then we require for the FE method approximately 9 hours and the RB method requires slightly more than 0.1 % of the FE compute time.

This demonstrates that the RB method is not only useful for large models but can be also helpful for small scale models if a very high number of simulations is necessary. One should only keep in mind that the smaller the model usually the more simulation runs it will take before it pays off to use the RB instead of the FE method. This pay-off behavior is also dependent on the complexity of the model. The Base model showed a similar number of simulations required for the RB method to be more efficient than the FE method, independent of the model size. The reason for this is that we needed only three basis functions. Hence, the construction of the basis was relatively cheap and we obtained similar computational savings for all model sizes.

Nonetheless, in all cases the number of runs is far below the thousands to millions of runs usually required for stochastical inversions, uncertainty quantification, etc. and the gained time for these types of applications is expected to be very high.

Another aspect is seen in Fig. 14 where we compare the performance for the RB and the standard FE method. In the case of the RB method, we obtain a strong scalability that varies, in case of the Base model, from 1.00 to 7.15 for 1 and 16 cores, respectively. The FE method has, for the same number of cores, a strong scalability changing between 1.00 and 1.37. For comparison, the ideal values for the strong scalability vary between 1.00 and 16.00. Consequently, the RB method shows a much stronger scalability than the FE method. Similarly, for the parallel efficiency, we get values between 1.00 and 0.45 for the RB method and from 1.00 to 0.09 for the FE method. This means that the RB method shows at all times a better performance than the FE method. Also, note that the difference in performance is larger for a smaller number of cores.

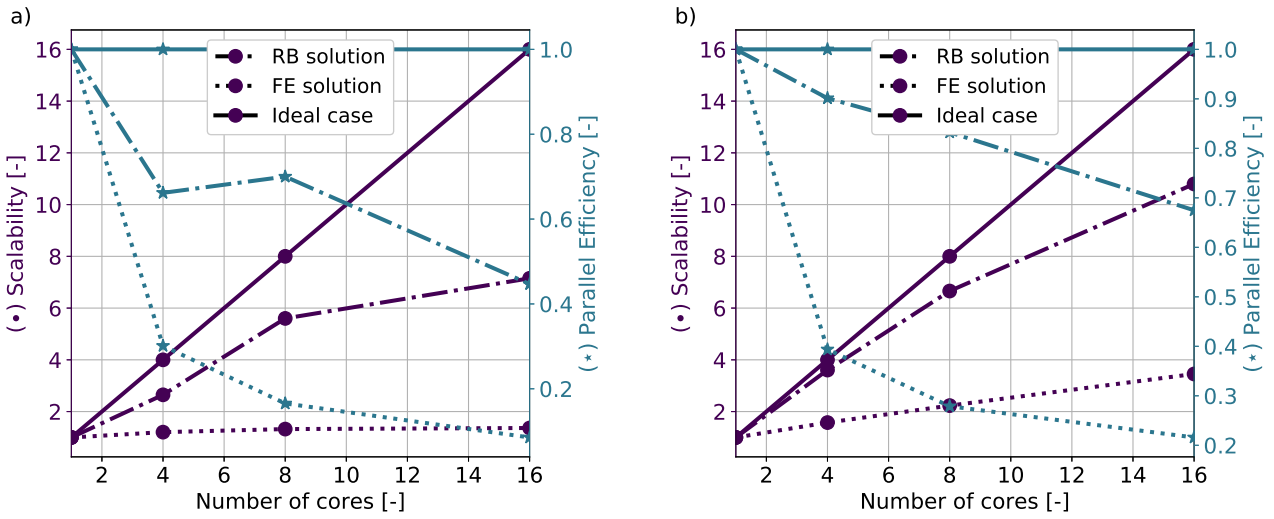


**Fig. 14** Performance analysis for the a) Base model (1,512,161 degrees of freedom) and b) Fault model (1,969,077 degrees of freedom). Shown are the strong scalability (purple lines) and the parallel efficiency (blue lines). The performance test has been done on IIntel Xeon E5-2680 v3 Haswell cores (2.5 GHz).

For geothermal conduction problems, we do not require the full capabilities of a standard HPC cluster due to the simplicity of the problem. Hence, we still have computing resources left that can be used to compensate for the additional time of the basis construction by using more cores. Using the provided MOOSE implementation, no additional work has to be invested to parallelize the problem since MOOSE offers a built-in parallelization that hides all MPI processes from the user.

Please note that the scaling test presented here uses the steady-state thermal conduction problems as a basis; this means that its physics is fairly simple. So, even for large model sizes, the problems are still fairly simple, and hence computationally not very intensive. Consequently, it is not ideal for scaling tests because few cores are sufficient to compute the problem. What we want to emphasize is that, for many-query problems, the RB method is more efficient than the FE method, a trend that is expected also for other problems that are more complex in terms of model geometry and the underlying physics.

A first indication that this is true is seen in Fig. 14b, where we did the same performance test for the Fault model. Here, we observe a slightly better performance of the RB method than for the Base model for up to 16 cores. The strong scalability increases from 7.15 to 10.80, and the parallel efficiency from 0.45 to 0.67, although the model has only 23 % more degrees of freedom.

Furthermore, the size of the training sample has, depending on the error bound used, an influence on the offline times. We used the dual residual norm to calculate the Riesz representor. The error bound applied here is thus relatively insensitive to the size of the training set. So, a general way to reduce the offline time is to choose a training set that is as small as possible. However, one needs to be careful that the training set is not too small. This would result in a significant accuracy loss because the domain is undersampled. The reason for that is that for constructing a new basis function we require one training parameter. In our example, it is, therefore, more important to have a training set that is large enough in order to avoid a recalculation than choosing a smaller training set. For the Base model, a small training set is enough, due to the low parameter complexity of the model. We performed simulations with a training size of 5, 100, and 1000 parameters using the Base model with 756,814 degrees of freedom. For this model, we got runtimes of 1,284.77 s (5 training parameters), 1,294.65 s (100 training parameters), and 1,285.9 s (1,000 training parameters). We would expect a slight increase in the computation times for more training parameters. However, the fluctuations due to different workloads of the cluster are in the same range as the increase in computation time, and are hence masked by these effects. The Fault model needs more training samples for our simulations because of the higher parameter complexity of the model.

We explained in Chapter 2 that the number of basis functions for the RB space is, among other things, determined by the user-defined error tolerance. This is advantageous for geoscientific applications since the measurement error we obtain largely varies for different methods and settings. By defining the error tolerance, we are able to adjust to this variety because having a slower but very accurate approximation of the FE space while having high measurement errors,

and vice versa is not beneficial at all. This means that we can take the measurement error minus a safety factor for the error tolerance, such that we get an optimal speed-up (as few basis functions as possible) without losing accuracy.

In Section 3, we already mentioned that we consider non-dimensional parameters only. This yields a better solver performance since the residuals are without dimensions. In the case of this geothermal example where the scales of the parameters are similar, this does not play a major role. However, if we additionally consider the pressure, for instance, it would have a significant influence since the scale differences between pressure and temperature are large. We considered the non-dimensional description especially because of the RB method. The error bound we used in our Greedy algorithm is sensitive to the mesh dimensions. Consequently, a consideration of the length in its dimensional form results in a high error bound which in turn leads to a premature termination of the Greedy algorithm, thus resulting in a lower approximation accuracy. This is especially true for geoscientific applications since our models generally have an extension of several hundreds of meters to several ten thousands of meters. Another reason to consider only non-dimensional variables are the Dirichlet boundary conditions. As in many other mathematical approaches, inhomogeneous (i.e., non-zero), Dirichlet boundary conditions are problematic. In contrast to, for instance, Neumann and Robin (natural) boundary conditions, the Dirichlet boundary conditions are so-called forced or essential boundary conditions. That means they do not appear in the integral (weak) form of the PDE but are later on enforced onto the system of equations. For the implementation of the RB method in libMesh, inhomogeneous Dirichlet boundary conditions yield inaccurate approximations due to the treatment of the affine decomposition. If we non-dimensionalize our problem instead such that the boundary is equal to zero (as done in this paper), we can resolve the problem.

Keep in mind that the issue with the Dirichlet boundary conditions is not a specific problem of the RB method but appears for several approaches. Hence, it is a good idea to consider a non-dimensional form to achieve i) a better solver performance and reduce numerical problems and ii) to gain a better performance of the method itself.

## 6 Outlook

As demonstrated throughout the paper the RB method is promising for real-time and many-query applications. For these reasons, we plan to use the developed code package for data assimilation problems, inversions, sensitivity analysis, and uncertainty quantifications. All these problems have in common that they require numerous forward simulations. We recently coupled the DwarfElephant package and the Dakota toolkit [2], developed by Sandia National Laboratories, in order to perform, for instance, inversions. Additionally, we saw that the method is powerful especially for large-scale models. Hence, we plan to test the methodology by using more complex large-scale real-case geological models. Furthermore, we already implemented the RB method for transient problems. In a next step, we want to investigate the behavior of the transient implementation in a geological context for both synthetic and real data. Furthermore, we plan to use the implementation presented here in the context of data assimilation problems.

**Acknowledgements** We would like to acknowledge the funding provided by the DFG through DFG Project GSC111. Furthermore, we like to thank two anonymous reviewers for helping to improve this paper through their useful remarks and comments. We also gratefully acknowledge the computing time granted through JARA-HPC on the supercomputer JURECA at Forschungszentrum Jülich.

This is a pre-print of an article published in Computational Geosciences. The final authenticated version is available online at: `https://doi.org/10.1007/s10596-019-09916-6`.

## References

1. Abdulle, A., Budáč, O.: A Petrov–Galerkin reduced basis approximation of the Stokes equation in parameterized geometries, Comptes Rendus Mathematique 353(7), 641–645 (2015).
2. Adams, B.M., Ebeida, M., Eldred, M., Geraci, G., Jakeman, J., Maupin, K., Monschke, J., Swiler, L., Stephens, J., Vigil, D., Wildey, T., Bohnhoff, W., Dalbey, K., Eddy, J., Frye, J., Hooper, R., Hu, K., Hough, P., Khalil, M., Ridgway, E., Rushdi, A.: Dakota, a multilevel parallel object-oriented framework for design optimization, parameter estimation, uncertainty quantification, and sensitivity analysis: Version 6.6 users manual. Sandia National Laboratories, Tech. Rep. SAND2014-4633 (2017)
3. Balay, S., Abhyankar, S., Adams, M.F., Brown, J., Brune, P., Buschelman, K., Dalcin, L., Eijkhout, V., Gropp, W.D., Kaushik, D., Knepley, M.G., May, D.A., McInnes, L.C., Rupp, K., Smith, B.F., Zampini, S., Zhang, H., Zhang, H.: PETSc Web page. http://www.mcs.anl.gov/petsc (2017)
4. Ballarin, F., Sartori, A., Rozza, G.: RBniCS-reduced order modelling in FEniCS. http://mathlab.sissa.it/rbnics (2017)
5. Brazell, O., Messenger, S., Abusalbi, N., Fjerstad, P.: Multicore evaluation and performance analysis of the eclipse and intersect reservoir simulation codes. In: Oil and Gas High Performance Computing Workshop (2010)
6. Cacace, M., Blöcher, G.: MeshIt - a software for three dimensional volumetric meshing of complex faulted reservoirs. Environmental Earth Sciences 74(6), 5191–5209 (2015)
7. Clapp, R.G., Fu, H., Lindtjorn, O.: Selecting the right hardware for reverse time migration. The leading edge 29(1), 48–58 (2010)
8. Curtis, A., Lomax, A.: Prior information, sampling distributions, and the curse of dimensionality. Geophysics 66(2), 372–378 (2001)
9. Floris, F., Bush, M., Cuypers, M., Roggero, F., Syversveen, A.R.: Methods for quantifying the uncertainty of production forecasts: a comparative study. Petroleum Geoscience 7(S), S87–S96 (2001)
10. Fu, H., Clapp, R.G., Lindtjorn, O.: Revisiting convolution and fft on parallel computation platforms. In: SEG Technical Program Expanded Abstracts 2010, pp. 3071–3075. Society of Exploration Geophysicists (2010)

11. Geuzaine, C., Remacle, J.F.: Gmsh: A 3-d finite element mesh generator with built-in pre-and post-processing facilities. International journal for numerical methods in engineering 79(11), 1309–1331 (2009)
12. Ghasemi, M., Gildin, E.: Model order reduction in porous median flow simulation using quadratic bilinear formulation. Computational Geosciences 20(3), 723–735 (2016)
13. Grepl, M.A., Patera, A.T.: A posteriori error bounds for reduced basis approximations of parametrized parabolic partial differential equations. ESAIM: Mathematical Modelling and Numerical Analysis 39(1), 157–181 (2005)
14. Hecht, F., Pironneau, O., Le Hyaric, A., Ohtsuka, K.: Freefem++. Numerical Mathematics and Scientific Computation. Laboratoire JL Lions, Université Pierre et Marie Curie, http://www.freefem.org/ff+ 3 (2007)
15. Herrmann, F.J., Friedlander, M.P., Yilmaz, O.: Fighting the curse of dimensionality: Compressive sensing in exploration seismology. IEEE Signal Processing Magazine 29(3), 88–100 (2012)
16. Hesthaven, J.S., Rozza, G., Stamm, B., et al.: Certified reduced basis methods for parametrized partial differential equations. SpringerBriefs in Mathematics, Springer (2016)
17. Huynh, D., Nguyen, N., Rozza, G., Patera, A.: Documentation for rbMIT Software: I. Reduced basis (RB) for Dummies. Massachusetts Institute of Technology, 2007-2010. http://augustine.mit.edu/methodology/methodology_rbMIT_System .htm
18. Cacace, M., Jacquey, A.: Flexible parallel implicit modelling of coupled thermal–hydraulic–mechanical processes in fractured rocks. Solid Earth 8(5), 921–941 (2017).
19. Jacquey, A., Cacace, M., Blöcher, G., Milsch, H., Deon, F.: From localized to homogeneous deformation of porous rocksinsights from laboratory experiments and numerical modelling. In: Geo-Proc 2017 Book of Abstracts: 6th International Conference on Coupled THMC Processes in Geosystems, p. 50
20. Jülich Supercomputing Centre: JURECA: General-purpose supercomputer at Jülich Supercomputing Centre. Journal of large-scale research facilities 2(A62) (2016). DOI 10.17815/jlsrf-2-121. URL http://dx.doi.org/10.17815/jlsrf-2-121
21. Jung, N.: Error Estimation for Parametric Model Order Reduction and Its Application. VDI Verlag (2012)
22. Kärcher, M., Tokoutsi, Z., Grepl, M.A., Veroy, K.: Certified reduced basis methods for parametrized elliptic optimal control problems with distributed controls. Journal of Scientific Computing pp. 1–32 (2017)
23. Kirk, B.S., Peterson, J.W., Stogner, R.H., Carey, G.F.: libmesh: a c++ library for parallel adaptive mesh refinement/coarsening simulations. Engineering with Computers 22(3–4), 237–254 (2006)
24. Knezevic, D.J., Peterson, J.W.: A high-performance parallel implementation of the certified reduced basis method. Computer Methods in Applied Mechanics and Engineering 200(13–16), 1455–1466 (2011). https://doi.org/10.1016/j.cma.2010.12.026
25. van Leeuwen, P.J.: Nonlinear data assimilation in geosciences: an extremely efficient particle filter. Quarterly Journal of the Royal Meteorological Society 136(653), 1991–1999 (2010)
26. Martini, I., Rozza, G., Haasdonk, B.: Reduced basis approximation and a-posteriori error estimation for the coupled Stokes-Darcy system. Advances in Computational Mathematics 41(5), 1131–1157 (2015)
27. Midttømme, K., Roaldset, E., Aagaard, P.: Thermal conductivity claystones and mudstones of selected from england. Clay Minerals 33(1), 131–145 (1998)
28. Milk, R., Rave, S., Schindler, F.: pymorgeneric algorithms and interfaces for model order reduction. SIAM Journal on Scientific Computing 38(5), S194–S216 (2016)
29. Poulet, T., Veveakis, M.: A viscoplastic approach for pore collapse in saturated soft rocks using redback: an open-source parallel simulator for rock mechanics with dissipative feedbacks. Computers and Geotechnics 74, 211–221 (2016)
30. Poulet, T., Veveakis, M., Paesold, M., Regenauer-Lieb, K.: REDBACK: An open-source highly scalable simulation tool for rock mechanics with dissipative feedbacks. In: AGU Fall Meeting Abstracts (2014)
31. Prud'homme, C., Rovas, D.V., Veroy, K., Machiels, L., Maday, Y., Patera, A.T., Turinici, G.: Reliable real-time solution of parametrized partial differential equations: Reduced-basis output bound methods. Journal of Fluids Engineering 124(1), 70–80 (2002)
32. Prud'homme, C., Chabannes, V., Doyeux, V., Ismail, M., Samake, A., Pena, G.: Feel++: A computational framework for galerkin methods and advanced numerical methods. In: ESAIM: Proceedings, vol. 38, pp. 429-5455. EDP Sciences (2012)
33. Quarteroni, A., Manzoni, A., Negri, F.: Reduced Basis Methods for Partial Differential Equations: An Introduction. UNITEXT. Springer International Publishing (2015)
34. Rizzo, C.B., de Barros, F.P., Perotto, S., Oldani, L., Guadagnini, A.: Adaptive pod model reduction for solute transport in heterogeneous porous media. Computational Geosciences pp. 1–12 (2017)
35. Rousset, M.A., Huang, C.K., Klie, H., Durlofsky, L.J.: Reduced order modeling for thermal recovery processes. Computational Geosciences 18(3–4), 401–415 (2014)
36. Tonks, M.R., Gaston, D., Millett, P.C., Andrs, D., Talbot, P.: An object-oriented finite element framework for multiphysics phase field simulations. Computational Materials Science 51(1), 20–29 (2012)
37. University of Stuttgart, University of Münster, University of Ulm, Sandia Lawrence Livermore National Research Laboratory: http://www.ians.uni-stuttgart.de/MoRePaS/software/rbmatlab/1.13.10/doc/index.html
38. de la Varga, M., Schaaf, A., Wellmann, F.: GemPy 1.0: open-source stochastic geological modeling and inversion. Geoscientific Model Development (2019)
39. Veroy, K., Patera, A.: Certified real-time solution of the parametrized steady incompressible navierstokes equations: rigorous reduced-basis a posteriori error bounds. International Journal for Numerical Methods in Fluids 47(8–9), 773–788 (2005)
40. Veroy, K., Prud'homme, C., Rovas, D.V., Patera, A.T.: A posteriori error bounds for reduced-basis approximation of parametrized noncoercive and nonlinear elliptic partial differential equations. In: Proceedings of the 16th AIAA computational fluid dynamics conference, vol. 3847, pp. 23–26. Orlando, FL (2003)
41. Volkwein, S.: Model reduction using proper orthogonal decomposition. Lecture Notes, Institute of Mathematics and Scientific Computing, University of Graz. see http://www. unigraz.at/imawww/volkwein/POD. pdf (2011)
42. Wellmann, J.F., Regenauer-Lieb, K.: Uncertainties have a meaning: Information entropy as a quality measure for 3-d geological models. Tectonophysics 526, 207–216 (2012)
43. Wellmann, J.F., Reid, L.B.: Basin-scale geothermal model calibration: Experience from the Perth Basin, Australia. Energy Procedia 59, 382–389 (2014)